Title

Sequence-independent recognition of the amyloid structural motif by GFP protein family

Journal

Proceedings of the National Academy of Sciences of the United States of America, 117(36)

ISSN

0027-8424

Authors

Xu, Sherry CS
LoRicco, Josephine G
Bishop, Anthony C
et al.

Publication Date

2020-09-08

DOI

10.1073/pnas.2001457117

Peer reviewed

Sequence-independent recognition of the amyloid structural motif by GFP protein family

Sherry C. S. Xu[a,b,1], Josephine G. LoRicco[a,b,1], Anthony C. Bishop[a,b,1], Nathan A. James[a,b], Welby H. Huynh[a,c], Scott A. McCallum[a], Nadia R. Roan[d,e], and George I. Makhatadze[a,b,c,2]

[a]Center for Biotechnology and Interdisciplinary Studies, Rensselaer Polytechnic Institute, Troy, NY 12180; [b]Department of Biological Sciences, Rensselaer Polytechnic Institute, Troy, NY 12180; [c]Department of Chemistry and Chemical Biology, Rensselaer Polytechnic Institute, Troy, NY 12180; [d]Department of Urology, University of California, San Francisco, CA 94158; and [e]Gladstone Institute of Virology and Immunology, San Francisco, CA 94158

Edited by Susan Marqusee, University of California, Berkeley, CA, and approved August 5, 2020 (received for review January 24, 2020)

Cnidarian fluorescent protein (FP) derivatives such as GFP, mCherry, and mEOS2 have been widely used to monitor gene expression and protein localization through biological imaging because they are considered functionally inert. We demonstrate that FPs specifically bind amyloid fibrils formed from many natural peptides and proteins. FPs do not bind other nonamyloid fibrillar structures such as microtubules or actin filaments and do not bind to amorphous aggregates. FPs can also bind small aggregates formed during the lag phase and early elongation phase of fibril formation and can inhibit amyloid fibril formation in a dose-dependent manner. These findings suggest caution should be taken in interpreting FP-fusion protein localization data when amyloid structures may be present. Given the pathological significance of amyloid-related species in some diseases, detection and inhibition of amyloid fibril formation using FPs can provide insights on developing diagnostic tools.

GFP-like proteins | amyloid fibril | binding | inhibition

Amyloids are protein aggregates that self-assemble into highly ordered fibrillar structures (1, 2). Amyloids came into prominence due to their association with a large number of human diseases (3, 4). Numerous neurodegenerative diseases have amyloid fibrils as characteristic biomarkers of the disease state. Alzheimer's disease is characterized by the formation of amyloid plaques — clumps of amyloid fibrils formed by the aggregation of the proteins Aβ1–40 and Aβ1–42 (5, 6). The aggregation of tau protein into amyloid fibrils is found in a class of related neurodegenerative diseases collectively known as "tauopathies" (7). Parkinson's disease features cerebellar amyloid aggregates of α-synuclein (8–10), and Huntington's disease has the hallmark of aggregated huntingtin (11–14). Beyond neurodegenerative disease, protein aggregation is associated with systemic amyloidosis (15, 16) and diabetes (17, 18). Amyloid fibrils have also been found to be factors in the transmission of infectious diseases. PAPf39 (a 39-residue peptide corresponding to residues 248–286 in human prostatic acidic phosphatase) and SEM1 (a 22-residue peptide corresponding to residues 86–107 in human semenogelin I protein) amyloid fibrils, both naturally occurring in human semen, have been found to increase infectivity of viruses including HIV (19). Thus, understanding the causes of protein aggregation is essential for the development of diagnostic tools and therapeutic agents to combat these widespread and growing health problems.

It is known that amyloid fibril formation in vitro follows a nucleation-dependent elongation mechanism, and the process is generally irreversible. However, due to the lack of adequate analytical methods, the detailed understanding of the structural features of various intermediates on the fibrillation pathway, including the structure and mechanism of nuclei formation, remains elusive. For example, the fluorescent dyes thioflavin T (ThT) and Congo Red (CR) are believed to be specific for the fibrillar structure but cannot report on the structural changes that occur during the nucleation phase of the fibrillation reaction.

In studying amyloid fibril formation using GFP (green fluorescent protein from *Aequorea victoria*) fusion proteins, we made the serendipitous discovery that GFP alone colocalized with amyloid fibrils. To examine how ubiquitous this was, we extended our studies to other cnidarian fluorescent proteins (FPs), mCherry, a monomeric derivative of dsRed protein from sea anemone *Discosoma sp.* and mEOS2, monomeric derivative of photoactivatable green to red fluorescent protein from stony coral *Lobophyllia hemprichii*, and probed their ability to bind over a dozen different amyloid fibrils. Here, we present evidence that FPs bind specifically to the core of various amyloid fibrils, and allows various intermediates on the fibrillation pathway to be visualized using fluorescence microscopy. We also find that FPs can bind early prefibrillar species along the fibrillation pathway and can inhibit amyloid fibril formation.

Results and Discussions

GFP Binding to Amyloid Fibrils Visualized by Confocal Fluorescence Microscopy. We formed amyloid fibrils from biologically relevant peptides and proteins (AβM1–40, AβM1–42, Aβ1–42, PAPf39, SEM1, IAPP, insulin, hen egg white lysozyme) as well as nonbiological materials such as catalytic (20) or chemical (21) fibrils and confirmed the presence of fibrillar material using atomic force

Significance

GFP and other related fluorescent proteins (FPs) are widely used in biological sciences. We discovered that FPs have an intrinsic high binding propensity for the core of amyloid fibrils. We have demonstrated this using over 10 different amyloid fibrils, characterized the binding interface, probed binding interface via mutagenesis, and performed a number of controls to show that binding is specific to amyloid structures and not to other nonamyloid fibrillar structures or soluble proteins with extended β-structure. This previously unrecognized functionality of FPs has two major implications: 1) It provides a tool to study amyloid structures, and 2) It suggests that caution should be taken when FPs are used as a fusion to visualize the cellular localization of proteins of interest.

Author contributions: S.C.S.X., J.G.L., A.C.B., and G.I.M. designed research; S.C.S.X., J.G.L., A.C.B., N.A.J., and W.H.H. performed research; S.A.M. and N.R.R. contributed new reagents/analytic tools; S.C.S.X., J.G.L., A.C.B., N.A.J., W.H.H., S.A.M., N.R.R., and G.I.M. analyzed data; and S.C.S.X., J.G.L., A.C.B., N.A.J., W.H.H., S.A.M., N.R.R., and G.I.M. wrote the paper.

Competing interest statement: S.C.S.X., J.G.L., A.C.B., N.A.J. and G.I.M. are inventors on a US Patent Application (PCT/US18/14770) that covers the use of FPs to detect amyloid fibrils.

This article is a PNAS Direct Submission.

[1]S.C.S.X., J.G.L., and A.C.B. contributed equally to this work.

[2]To whom correspondence may be addressed. Email: makhag@rpi.edu.

This article contains supporting information online at https://www.pnas.org/lookup/suppl/doi:10.1073/pnas.2001457117/-/DCSupplemental.

First published August 24, 2020.

microscopy (AFM) (Fig. 1 *A* and *B* and *SI Appendix*, Fig. S1). The presence of fibrillar material can also be visualized by confocal fluorescence microscopy (CFM) in the presence of the traditional amyloid binding chemical dyes thioflavin T (ThT) and Congo Red (CR) (Fig. 1*A*). When these fibrillar structures were imaged by CFM in the presence of GFP, mCherry (Fig. 1 *A* and *B* and *SI Appendix*, Fig. S1), or mEOS2 (*SI Appendix*, Fig. S2), we also detected significant binding of the FP proteins to the fibrils. To show that FPs bind specifically to fibrillar structures and not to corresponding monomers, we performed a dot blot experiment (Fig. 1*C*). In these experiments, fibrils or the corresponding monomeric form of the amyloidogenic polypeptides were spotted onto a nitrocellulose membrane, exposed to an FP, and imaged by fluorescence microscopy. Only fibrillar structures showed binding of GFP or mCherry (Fig. 1*C* and *SI Appendix*, Fig. S3). These results suggest that FPs bind specifically to amyloid fibrils of these peptides.

Some amyloid fibrils made of larger proteins have a "fuzzy coat" around them, formed by unstructured parts of the protein that are not involved in the formation of the amyloid core. Two proteins, tau and α-synuclein (α-syn), form such coated fibrillar structures (22). We found that GFP fails to bind such fibrils as evident by CFM imaging (Fig. 1 *D* and *E*). However, if the tau and α-syn fibrils were pretreated with a nonspecific protease (subtilisin) that removes this "fuzzy coat," then binding was detected (Fig. 1 *D* and *E*). To further confirm that the presence of a "fuzzy coat" prevents recognition of the amyloid core of tau by GFP, we used two truncated tau constructs, K18 and K19 (23). K18 and K19 lack N- and C-terminal unstructured sequences, which form the "fuzzy coat" (Fig. 1*F*), but retain the ability to form amyloid fibrils. Importantly, both K18 and K19 amyloid fibrils show GFP binding by CFM imaging in the absence of subtilisin treatment (Fig. 1*G*). These findings suggest that FPs are proteins that specifically recognize the amyloid core of the fibrillar structures.

GFP Binds Amyloid Fibrils with High Affinity. We next quantified the macroscopic kinetic and thermodynamic parameters of GFP binding to amyloid fibrils. To this end, we visualized the binding of GFP to fibrillar structures by time-resolved total internal reflection fluorescence (TIRF) microscopy. TIRF microscopy of individual PAPf39 amyloid fibrils shows that GFP molecules freely move around while dynamically binding and unbinding the fibrillar material (Movie S1). Quantitative analysis of the TIRF data allows estimates of kinetic parameters for binding $k_{on} = 0.027 \pm 0.02\ s^{-1}{\cdot}nM^{-1}$ and $k_{off} = 0.62 \pm 0.04\ s^{-1}$ (*SI Appendix*, Fig. S4). The macroscopic apparent equilibrium binding constant (intrinsic binding constant of GFP per site) estimated from the kinetic constants was $K_b = k_{off}/k_{on} = 23 \pm 5$ nM. This rather high affinity also supports the notion of high specificity of GFP binding to amyloids fibrils.

GFP Does Not Bind Nonamyloid Fibrillar or Extended β-Sheet Structures. We next sought to examine whether FPs can bind nonamyloid

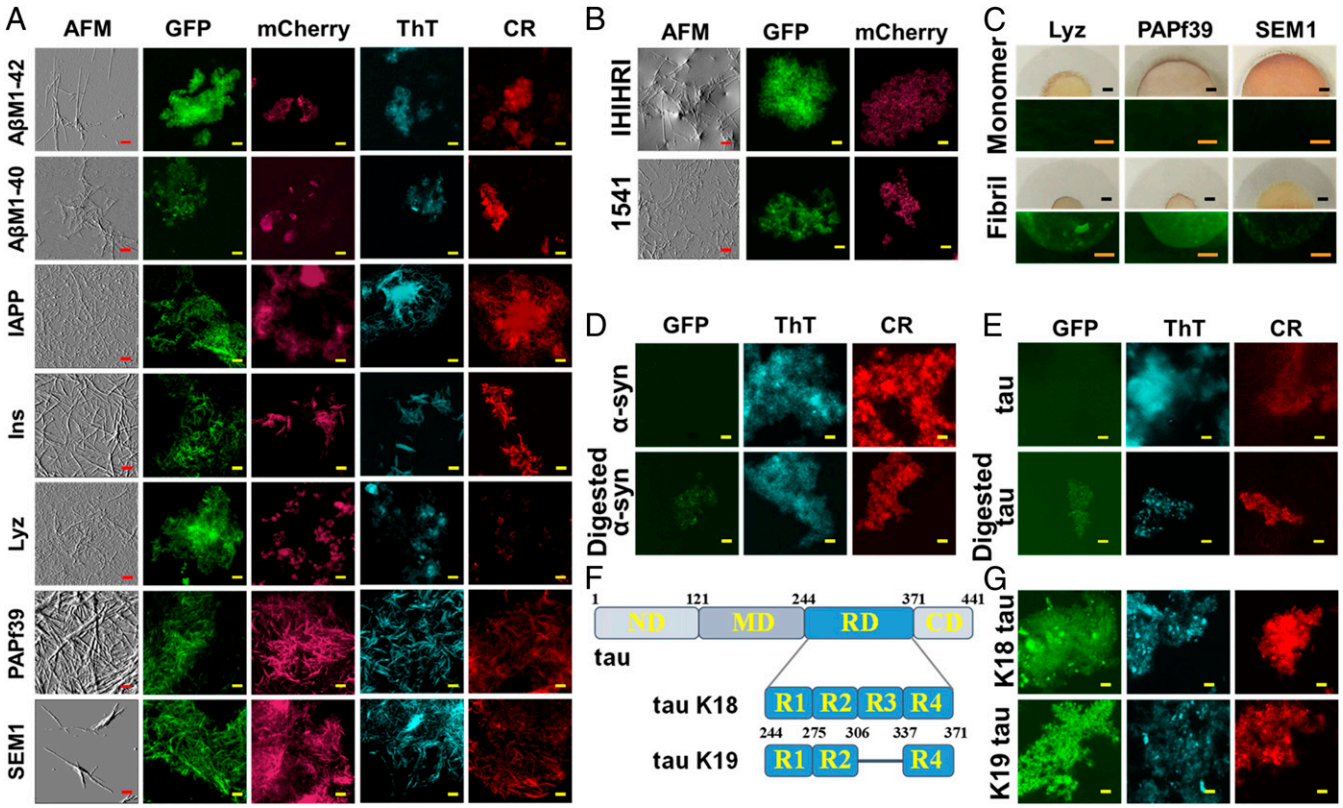

Fig. 1. GFP and mCherry bind various amyloid fibrils. (*A*) Biological amyloid fibrils: AFM images (column 1) show the presence of amyloid fibrils in all samples. CFM (columns 2–5) images of 90 μg/mL amyloid fibrils in the presence of 5 μM GFP (column 2), 5 μM mCherry (column 3), 50 μM ThT (column 4), and 50 μM CR (column 5). (*B*) Nonbiological amyloid fibrils: AFM images of fibrils made of synthetic heptapeptide or the small-molecule-derived chemical fibril 1541. Both of these nonbiological amyloid fibrils can bind GFP and mCherry as seen from CFM images. See also *SI Appendix*, Fig. S1. (*C*) Dot blot experiments show that GFP binds to amyloid fibrils but not to their corresponding monomeric peptides. *Upper*, silver staining, *Lower*, GFP staining. See also *SI Appendix*, Fig. S3. (*D* and *E*) GFP binds to α-synuclein or full-length tau only after their "fuzzy coats" were removed by treatment with nonspecific protease subtilisin. (*F* and *G*) The amyloid fibrils made of tau variants K18 and K19 (i.e., that contain only amyloid core forming repeat domains) do not require treatment with subtilisin to bind GFP. (Scale bars: AFM: *A* and *B*, 500 nm; CFM: *A*, *B*, and *D*–*G*, 5 μm; *C*: silver staining, 1 mm; *C*: GFP staining, 0.5 mm.)

fibrillar structures. Protein-based fibrillar structures that are not amyloids, such as microtubules or actin filaments, showed no detectable binding (Fig. 2*A*). To further probe the specificity of FPs for amyloid fibrils, we examined the ability of FPs to bind another form of protein aggregate, the amorphous aggregate. We used amorphous aggregates (24) formed by IgG and BSA and found that GFP did not bind to either (Fig. 2*B*), supporting the previous conclusion that these FPs are specific to amyloid fibrils and not to other types of protein aggregates. Interestingly, ThT and CR, chemical dyes that are believed to be specific to amyloid fibrils, both bound to the amorphous IgG and bovine serum albumin (BSA) aggregates (Fig. 2*C*). Finally, we asked if GFP can bind proteins that contain extended β-sheet structures. For these experiments, we examined pertactin and OspA proteins in sedimentation velocity experiments, in which protein–protein interactions can be detected by an increase in sedimentation coefficient of GFP in the presence of protein of interest. The sedimentation coefficient of GFP alone or in the presence of pertactin or OspA does not change, suggesting no detectable binding (Fig. 2*D*). This result provides further support to the notion that that FPs bind not just any β-structure but specifically cross-β amyloid structures.

GFP Bind Various Species on Fibrillation Pathway and Inhibits Fibrillation. Next, we sought to test whether GFP can bind other intermediate species along the fibrillation pathway. For this we periodically removed aliquots of fibrillation reaction at defined time points and following the addition of GFP, imaged the solution using CFM (*SI Appendix*, Fig. S5). The CFM images were collected over a relatively large area (900 μm × 900 μm) to generate a statistically meaningful dataset (Fig. 3*A*). In parallel, we monitored fibrillation using the traditional method of monitoring the changes in bulk fluorescence from CR (Fig. 3*A*) or ThT (*SI Appendix*, Fig. S5). CFM images showed the appearance of detectable particles already after 1 h into the fibrillation reaction when no CR or ThT signal increase was yet been observed. To quantify the time-dependent distribution of intensities in particles of different sizes, we have binned them into three groups: small identifiable particles (SIPs) with sizes less than 25 μm^2; medium identifiable particles (MIPs) with sizes between 25 μm^2 and 75 μm^2; and large identifiable particles (LIPs) with sizes larger than 75 μm^2. The time-dependent histogram shows the appearance of SIPs early in the kinetic pathway with no detectable MIPs or LIPs (Fig. 3*B*). As time progressed, the fraction of SIPs decreased, while the fraction of MIPs started to increase, reaching a maximum at ∼20 h. Importantly, the fraction of LIPs, appearing at later time points, coincides with the increase in bulk fluorescence signal from CR (Fig. 3*B*). These experiments suggest that GFP can bind not only mature fibrils but also smaller nonmonomeric species populated during the lag phase of the fibrillation reaction.

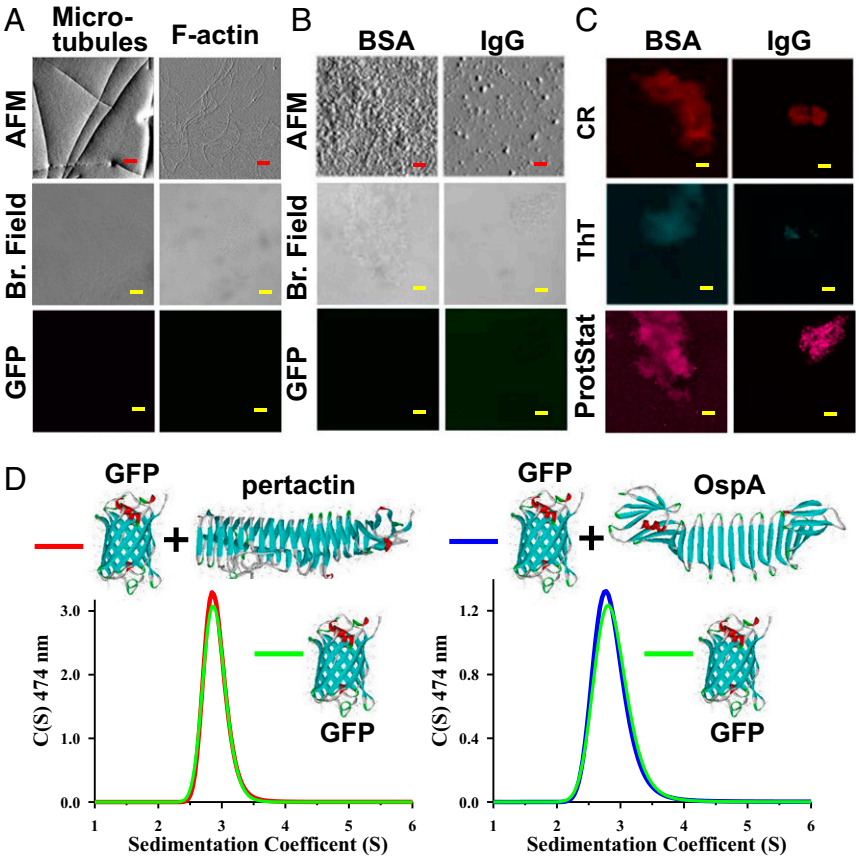

Fig. 2. GFP does not bind nonamyloid fibrils, amorphous aggregates, and proteins with extended β-sheet structures. (*A*) Tubulin and actin form fibrillar structure (microtubules and F-actin, see AFM images in row 1), these fibrillar structures are visible in bright field images in solution (row 2) but do not show staining with GFP (row 3). (*B* and *C*) Amorphous aggregates of IgG and BSA do not show fibrillar structure in AFM imaging, are visible in bright field images in solution but do not show staining with GFP, but are stained by ThT and CR. (Scale bars: *A*–*C*: AFM, 500 nm; CFM, 5 μm.) Note that images corresponding to bright field, GFP, and Proteostat (ProtStat) are images of the same field of view. (*D*) Soluble monomeric proteins pertactin and OspA that have extended β-sheet structure do not bind GFP as can be seen from comparing sedimentation velocity experiments of GFP alone and in the presence of pertactin and OspA (*SI Appendix*, Fig. S10). Cartoon representation of structures of GFP (PDB ID code: 2B3P), pertactin (PDB ID code: 1DAB) and OspA (PDB ID code 2OY7) are shown on the same scale.

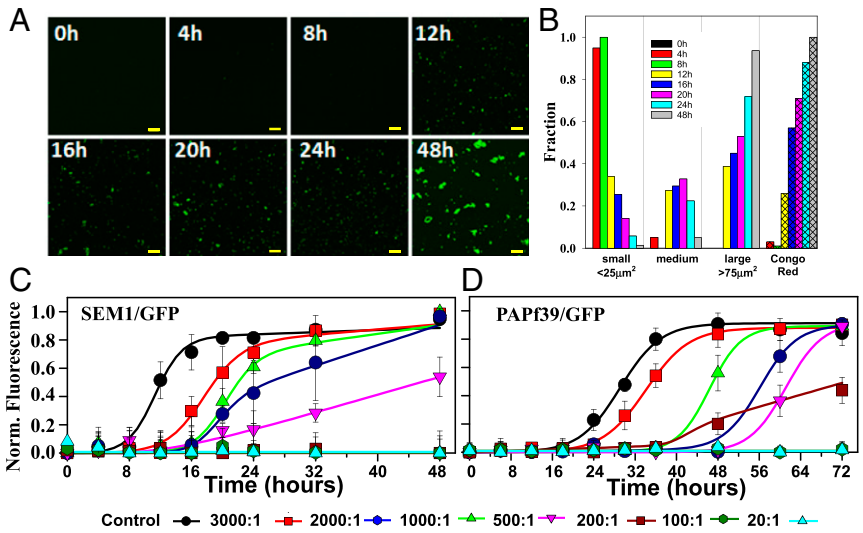

Fig. 3. Use of GFP to monitor kinetics of amyloid fibril formation. (*A* and *B*) CFM images monitoring kinetics of fibril formation as a function of time for 1.0 mg/mL SEM1 peptide. (Scale bar: 100 μm.) For these experiments, aliquots from the reaction were mixed with 5 μM GFP in PBS and 10 × 10 grid of CFM images covering 900 μm × 900 μm area were acquired. In parallel, bulk changes in CR fluorescence were monitored (*SI Appendix*, Fig. S5*A*). CFM images were analyzed by binning particles by size: SIPs < 25 μm^2, MIPs > 25 μm^2 and <75 μm^2, and LIPs > 75 μm^2. Notably, distributions of LIPs and CR overlap. See *SI Appendix*, Fig. S5*B* for reproducibility and ThT-based monitoring of fibrillation kinetics. (*C* and *D*) GFP shows dose-dependent inhibition of the amyloid fibril formation for SEM1 and PAPf39 amyloid fibrils. The concentration of the peptide in all reactions is 1 mg/mL. The different colors correspond to the ratios of the molar concentration of peptide monomer to the molar concentration of GFP. Data are shown as mean ± SD of triplicate experiments and the lines are drawn to guide the eye.

We next asked whether the interactions of FPs with smaller particles can modulate the kinetics of fibrillation. For these experiments, GFP/mCherry was added to the fibrillation reaction at the beginning (i.e., time 0; see *SI Appendix*, Fig. S6*A*) and the fibrillation was monitored by ThT/CR bulk fluorescence assay (Fig. 3 *C* and *D* and *SI Appendix*, Fig. S6 *B* and *C*) and CFM imaging (*SI Appendix*, Fig. S7). It is evident that GFP/mCherry inhibits fibrillation kinetics in a dose-dependent manner. Importantly, complete inhibition occurs at super substoichiometric ratios, suggesting binding to the small oligomeric species. Additional evidence for binding of GFP to species formed during the lag-phase comes from time-point inhibition assays (*SI Appendix*, Fig. S8*A*). For these experiments, GFP was added to the fibrillation reaction at different time points of fibrillation reaction and fibrillation was monitored by CR bulk fluorescence assay (*SI Appendix*, Fig. S8*B*). Addition of GFP early in the lag phase produced complete inhibition, while addition late in the lag phase led to a longer lag phase. Importantly, addition of GFP during the elongation phase of the reaction did not inhibit the fibrillation, suggesting GFP binding to elongating fibrils does not prevent monomer addition.

GFP Binds Amyloid Fibrils in a Preferred Orientation. To answer the question of whether GFP binding on the amyloid fibrils occurs in a particular fixed orientation relative to the fibril axis, we used fluorescence polarization microscopy. Solution containing fibrils in the presence of GFP or Proteostat (a dye that is similar in structure to a ThT dimer but has fluorescence properties that allow coimaging with GFP) was imaged with vertically or horizontally polarized light. The integrated fluorescence intensity ratios of the two images were plotted as a function of fibril angle from horizontal (*SI Appendix*, Fig. S9). It is known that the Proteostat dipole moment is aligned with the fibrillar axis (25), in agreement with our measurements. Since GFP shows a profile just opposite to that of Proteostat, the dipole moment of the GFP chromophore is perpendicular to the fibril axis. The direction of the electronic transition dipole moment relative to the molecular axis of GFP has been established (26) and is consistent with a parallel orientation of β-sheets of the GFP barrel to the amyloid cross-beta structure. More importantly, it implies that GFP adopts a fixed orientation on the amyloid fibril.

Mapping Amyloid Binding Surface on GFP. We next sought to map the surface of the GFP molecule that is involved in binding the fibrillar core. To this end, we performed paramagnetic relaxation enhancement (PRE) NMR experiments (27). In these experiments, the proximity of residues on the interface can be detected by an increase in nuclear relaxation rates due to the presence of a paramagnetic center. PAPf39 fibrils incorporating the paramagnetic probe (*Materials and Methods*) were mixed with GFP, and paramagnetic relaxation enhancement of GFP chemical shifts was measured (Fig. 4*A*). The resonances that experienced the largest PRE were mapped onto the three-dimensional structure of GFP (Fig. 4*B*). We found that the majority of PREs mapped to one face of the GFP β-barrel consisting of β-sheets 7 through 10. This face of GFP does not show any obvious physico-chemical properties except that it contains three surface Tyr residues that line up to form a row perpendicular to the direction of the β-strands (Fig. 4*B*). Considering that most amyloid-binding dyes contain phenolic groups, we hypothesized that this row of Tyr is important for the GFP binding to the fibrils. To test this hypothesis, we substituted these three Tyr residues with Ala to make nsaGFP (no surface aromatics) and probed this GFP variant in fibril inhibition assay (Fig. 4*C*). The nsaGFP had significantly lower inhibitory activity than WT GFP, suggesting that the Tyr row is important in modulating GFP interactions and, thus, indirectly supporting the mapping of GFP interface for amyloid fibrils using PRE NMR. We further tested the requirements for having Tyr residues at these positions by replacing them with Phe residues (i.e., keeping the aromatic moiety without the hydroxyl group, fsaGFP) and observed lower inhibition similar to nsaGFP (Fig. 4*C*). Moving the Tyr row to adjacent positions on the same face of GFP in the background of nsaGFP resulted in recovery of the inhibitory activity (nsaGFP+4Y), while adding two rows of Tyr residues on the

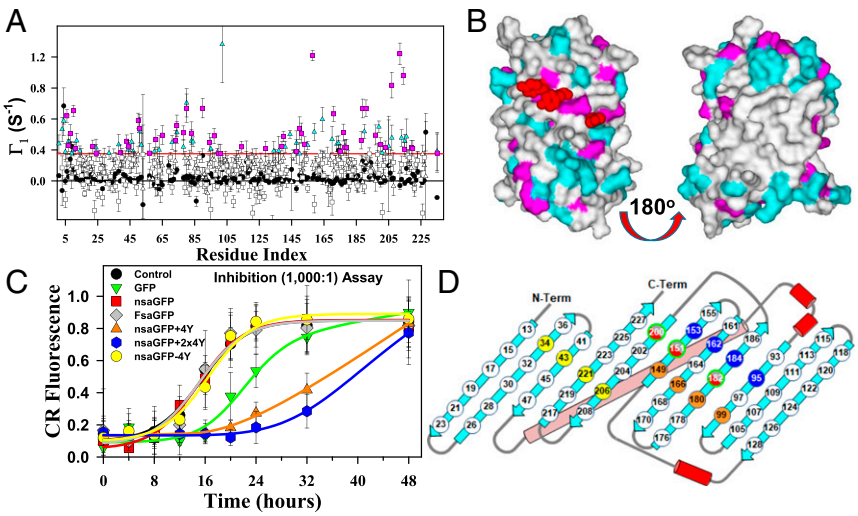

Fig. 4. Mapping of amyloid binding interface on GFP. (*A*) Experimentally derived NMR PREs are plotted as a function of the residue number of GFP: GFP in the presence of spin-labeled PAPf39 monomer (circles) or PAPf39 amyloid fibrils (triangles and squares). Red line shows the cutoff value based on GFP alone; open symbols show the signal below threshold, and cyan triangles and pink squares are for the values above threshold obtained from two different independent experiments using different labeling schemes. (*B*) Mapping the residues with a PRE above threshold on the structure of GFP (PDB ID code: 2B3P). Surface Tyr residues are shown as red CPK models, while cyan and pink colored surfaces correspond to the residues with PRE above threshold from two independent experiments identified in *A*. (*C*) Comparison of the inhibitory activity of GFP variants with different locations of Tyr row. All experiments are performed at 1,000:1 molar ratios of SEM1 to GFP. (*D*) Schematic rollout structure of GFP with the location of the surface mutations using the same color-coding as in *C*.

same face (nsaGFP+2 × 4Y) augmented the inhibitory effect. Interestingly, placing the Tyr row on the opposite side of the GFP surface (nsaGFP-4Y) had an inhibitory effect similar to that of nsaGFP (Fig. 4*C*). These experiments suggest that the Tyr row on a defined face of GFP can modulate binding. However, removal of the Tyr row does not completely abolish the binding, suggesting that other residues on the same face of GFP contribute to the interactions with the amyloid fibrils.

Conclusions

In conclusion, we have provided evidence that GFP, mCherry, and mEOS2 specifically bind amyloid fibrils. This suggests that protein localization imaging studies should avoid use of FP-fusion proteins if amyloid structures are known to be present. Furthermore, considering that there are many GFP and mCherry derivatives with different photophysical properties (excitation/emission wavelength, quantum yield), our findings suggest that FPs may be broadly useful as tools to study structural, thermodynamic, kinetic, and morphological aspects of amyloid fibril formation.

Materials and Methods

Peptides used in this work were synthesized using standard Fmoc chemistry. Proteins used in this work were expressed in *Escherichia coli* BL21(DE3) strain. Detailed methods, including protein and peptide purification, biophysical and biochemical assays, and NMR assignments, are available in *SI Appendix*.

Data and Materials Availability. All data are available in the main text or the supplementary materials, and plasmids generated specifically for this work are available upon request. All other data are available from the corresponding author upon reasonable request.

ACKNOWLEDGMENTS. We thank R. Linhardt, S. Koide, D. Eliezer, C. Bystroff, P. Klein, L. Looger, D. Walsh, and H. Lashuel for plasmids. We thank S. Gilbert, D. Swank, I. Korendovych, P. Tessier, O. Julien, J. Wells, P. Clark, and D. Raleigh for proteins, peptides, and chemical reagents. We thank S. Forth for use of TIRF microscope. We thank A. Crofoot, E. Nolan, J. Grossman, A. Tiwari, C. Moustouka, A. Schneggenburger, J. Morgan, S. Pryshchep, and M. Lopez for technical assistance. J.G.L. was supported by NIH Training Grant T32 GM067545. W.H.H. was supported by NIH Training Grant T32 AG057464. N.R.R. was supported by NIH Grants AI131374 and HD055764.

1. F. Chiti, C. M. Dobson, Protein misfolding, functional amyloid, and human disease. *Annu. Rev. Biochem.* **75**, 333–366 (2006).
2. L. Goldschmidt, P. K. Teng, R. Riek, D. Eisenberg, Identifying the amylome, proteins capable of forming amyloid-like fibrils. *Proc. Natl. Acad. Sci. U.S.A.* **107**, 3487–3492 (2010).
3. J. N. Buxbaum, R. P. Linke, A molecular history of the amyloidoses. *J. Mol. Biol.* **421**, 142–159 (2012).
4. F. Chiti, C. M. Dobson, Protein misfolding, amyloid formation, and human disease: A summary of progress over the last decade. *Annu. Rev. Biochem.* **86**, 27–68 (2017).
5. C. L. Masters *et al*., Amyloid plaque core protein in Alzheimer disease and Down syndrome. *Proc. Natl. Acad. Sci. U.S.A.* **82**, 4245–4249 (1985).
6. A. Alzheimer, R. A. Stelzmann, H. N. Schnitzlein, F. R. Murtagh, An English translation of Alzheimer's 1907 paper, "Uber eine eigenartige Erkankung der Hirnrinde". *Clin. Anat.* **8**, 429–431 (1995).
7. K. Iqbal, F. Liu, C. X. Gong, Tau and neurodegenerative disease: The story so far. *Nat. Rev. Neurol.* **12**, 15–27 (2016).
8. M. Goedert, Alpha-synuclein and neurodegenerative diseases. *Nat. Rev. Neurosci.* **2**, 492–501 (2001).
9. V. M. Lee, M. Goedert, J. Q. Trojanowski, Neurodegenerative tauopathies. *Annu. Rev. Neurosci.* **24**, 1121–1159 (2001).
10. M. G. Spillantini *et al*., Alpha-synuclein in Lewy bodies. *Nature* **388**, 839–840 (1997).
11. A. H. Schapira, C. W. Olanow, J. T. Greenamyre, E. Bezard, Slowing of neurodegeneration in Parkinson's disease and Huntington's disease: Future therapeutic perspectives. *Lancet* **384**, 545–555 (2014).
12. B. Dehay *et al*., Targeting α-synuclein for treatment of Parkinson's disease: Mechanistic and therapeutic considerations. *Lancet Neurol.* **14**, 855–866 (2015).
13. S. D. Kim, V. S. Fung, An update on Huntington's disease: From the gene to the clinic. *Curr. Opin. Neurol.* **27**, 477–483 (2014).
14. A. D. Ha, V. S. Fung, Huntington's disease. *Curr. Opin. Neurol.* **25**, 491–498 (2012).
15. M. Stoppini, V. Bellotti, Systemic amyloidosis: Lessons from β2-microglobulin. *J. Biol. Chem.* **290**, 9951–9958 (2015).
16. J. D. Gillmore, P. N. Hawkins, Pathophysiology and treatment of systemic amyloidosis. *Nat. Rev. Nephrol.* **9**, 574–586 (2013).
17. D. Raleigh, X. Zhang, B. Hastoy, A. Clark, The β-cell assassin: IAPP cytotoxicity. *J. Mol. Endocrinol.* **59**, R121–R140 (2017).

18. T. P. Knowles, M. Vendruscolo, C. M. Dobson, The amyloid state and its association with protein misfolding diseases. *Nat. Rev. Mol. Cell Biol.* **15**, 384–396 (2014).
19. J. Münch *et al*., Semen-derived amyloid fibrils drastically enhance HIV infection. *Cell* **131**, 1059–1071 (2007).
20. C. M. Rufo *et al*., Short peptides self-assemble to produce catalytic amyloids. *Nat. Chem.* **6**, 303–309 (2014).
21. O. Julien *et al*., Unraveling the mechanism of cell death induced by chemical fibrils. *Nat. Chem. Biol.* **10**, 969–976 (2014).
22. S. Wegmann, I. D. Medalsy, E. Mandelkow, D. J. Müller, The fuzzy coat of pathological human Tau fibrils is a two-layered polyelectrolyte brush. *Proc. Natl. Acad. Sci. U.S.A.* **110**, E313–E321 (2013).
23. P. Barré, D. Eliezer, Structural transitions in tau k18 on micelle binding suggest a hierarchy in the efficacy of individual microtubule-binding repeats in filament nucleation. *Protein Sci.* **22**, 1037–1048 (2013).
24. A. L. Fink, Protein aggregation: Folding aggregates, inclusion bodies and amyloid. *Fold. Des.* **3**, R9–R23 (1998).
25. M. R. Krebs, E. H. Bromley, A. M. Donald, The binding of thioflavin-T to amyloid fibrils: Localisation and implications. *J. Struct. Biol.* **149**, 30–37 (2005).
26. F. I. Rosell, S. G. Boxer, Polarized absorption spectra of green fluorescent protein single crystals: Transition dipole moment directions. *Biochemistry* **42**, 177–183 (2003).
27. G. M. Clore, Practical aspects of paramagnetic relaxation enhancement in biological macromolecules. *Methods Enzymol.* **564**, 485–497 (2015).